American Mineralogist, Volume 92, pages 1087–1092, 2007

Crystal-chemistry of Ni in marine ferromanganese crusts and nodules

Caroline L. Peacock and David M. Sherman*

University of Bristol, Department of Earth Sciences, Bristol BS8 1RJ, U.K.

Abstract

Marine ferromanganese crusts and nodules are highly enriched in transition metals such as Ni and Co, yet the crystal chemistry and mode of incorporation of these metals is poorly known. We characterized the crystal chemistry of Ni in two hydrogenetic Pacific ocean ferromanganese crust samples and a hydrogenetic nodule from the Madeira abyssal plain. Energy dispersive spectrometry shows that Ni is associated with the manganese oxide phases, in agreement with previous work. X-ray diffraction patterns show that the dominant $Mn^{3+/4+}$ oxide is a phyllomanganate similar to hexagonal birnessite or δ-MnO_2. Extended X-ray absorption fine-structure spectroscopy shows that the coordination environment of Ni results from structural incorporation into the phyllomanganate phase by replacement of $Mn^{3+/4+}$. In contrast, Ni initially sorbs to freshly prepared synthetic birnessite by surface complexation over vacancy sites in the MnO_2 layer. We propose that the transformation of Ni sorption from surface complexation to structural incorporation provides a potentially irreversible sink for Ni in seawater.

Keywords: Nickel, ferromanganese, hexagonal birnessite, goethite, adsorption, solid solution, scanning electron microscopy, EXAFS spectroscopy

Introduction

The concentration of Ni in marine ferromanganese deposits, deep-sea sediments, and seawater can be strongly controlled by sorption onto $Mn^{3+/4+}$ and Fe^{3+} (hydr)oxides (e.g., Goldberg 1954). Chemical analyses of Pacific Ocean ferromanganese nodules show a positive Ni-Mn correlation (e.g., Goldberg 1954; Willis and Ahrens 1962; Cronan 1969; Calvert and Price 1977). Several more recent sequential analysis studies have also shown a Ni-Mn association in Indian and Atlantic nodules (Moorby and Cronan 1981), in Pacific nodules and encrustations (Aplin and Cronan 1985), and in Pacific crusts (Koschinsky and Halbach 1995; Koschinsky and Hein 2003). Nickel-manganese spatial correlations have also been found with energy dispersive spectrometry (EDS) of Pacific nodules (e.g., Lei and Boström 1995) and Indian Ocean nodule and crust samples (e.g., Kumar et al. 1994; Dutta et al. 2001).

The association of Ni with Mn has been explained using the adsorption model of James and Healy (1972) (e.g., Li 1982; Koschinsky and Halbach 1995; Koschinsky and Hein 2003). This model assumes that metals sorb to mineral surfaces via purely electrostatic outer-sphere mechanisms. Nickel forms mainly hydrated divalent Ni^{2+} in seawater (e.g., Turner et al. 1981) and the model predicts that Ni^{2+} would be preferentially bound to the negative surface of MnO_2 ($pH_{PZC} = 2.3 \pm 0.2$, Catts and Langmuir 1986). In the past 15 years, however, spectroscopic evidence has emerged that metals sorb to Fe and Mn oxides by forming inner-sphere surface complexes (Brown and Parks 2001 and references therein). Moreover, sorption might also occur via structural incorporation and replacement of Fe^{3+} or $Mn^{3+/4+}$. Understanding the sorption mechanism is necessary before we can develop a thermodynamic model of trace-metal uptake. Even a qualitative understanding of the sorption mechanism can enable us to predict if trace metal-sorption is reversible (e.g., outer-sphere complexation) or irreversible (structural incorporation).

Extended X-ray absorption fine structure (EXAFS) spectroscopy can be used to investigate the coordination environment of Ni and, hence, if Ni is sorbed to Mn oxide phases via outer-sphere surface complexes, inner-sphere surface complexes, or structural incorporation. To our knowledge, there are no EXAFS studies of Ni associated with Mn in deep-sea ferromanganese deposits. However, EXAFS spectra have shown that divalent cations can adsorb above/below vacancy sites in the octahedral layers of synthetic hexagonal birnessite (e.g., Manceau et al. 2002a). However, EXAFS spectra of Ni in MnO_2-$Al(OH)_3$ mixed-layer lithiophorite in soil ferromanganese nodules show isomorphic substitution of Ni^{2+} for $Mn^{3+/4+}$ (Manceau et al. 2002b, 2005) and EXAFS spectra of Ni^{2+} in Co-Ni absolane show the formation of an intercalated $Ni(OH)_2$ layer (Manceau et al. 1992). Recently, we have found that Ni^{2+} sorbs to synthetic hexagonal birnessite (Hx-birnessite) by surface complexation over vacancy sites in the MnO_2 layer; however, Ni^{2+} sorbs to synthetic triclinic birnessite (Tc-birnessite) by forming surface complexes on edge sites of the MnO_2 layers (Peacock and Sherman 2007).

Ferromanganese nodules and crusts consist of a variety of $Mn^{3+/4+}$ oxides (such as δ-MnO_2, birnessite, and todorokite) and Fe^{3+} hydroxides (such as goethite). The structures of these minerals are based on sheets and chains of MnO_6 and FeO_6 octahedra, respectively (e.g., Burns and Burns 1977). Todorokite is a tunnel Mn oxide with diagnostic X-ray diffraction (XRD) peaks at ~10

* E-mail: dave.sherman@bris.ac.uk

0003-004X/07/0007–1087$05.00/DOI: 10.2138/am.2007.2378

and ~4.8 Å. Manganese minerals with this 3-D structure are also referred to as "10 Å-manganite" (e.g., Usui 1979). Manganese oxides with XRD peaks at ~7, 3.6, 2.4, and 1.4 Å are referred to as 7 Å manganite/manganate, birnessite, or δ-MnO_2. However, δ-MnO_2 has also been used to refer to Mn oxides that only show XRD peaks at ~2.4 and ~1.4 Å. In addition, the hydrated form of the ~7 Å manganate has a 10 Å layer spacing and is referred to as 10-Å buserite (Giovanoli 1980). In keeping with most recent studies (e.g., Villalobos et al. 2003), we refer to Mn minerals with ~7 and ~3.6 Å peaks as birnessite, and Mn minerals with ~2.4 and ~1.4 Å peaks only as δ-MnO_2. Additionally, birnessite can have a triclinic (Tc-birnessite) or hexagonal (Hx-birnessite) structure where Hx-birnessite possesses octahedral vacancies in the phyllomanganate layers (Drits et al. 1997). For hexagonal symmetry, the (100) and (110) reflections (corresponding to the XRD peaks at ~2.4 and ~1.4 Å, respectively) must show $d_{100}/d_{110} = \sqrt{3}$. Most natural birnessites (cf. Jones and Milne 1956; McKenzie 1989; Post 1992) and synthetic δ-MnO_2 (Villalobos et al. 2003) have hexagonal structures. In fact, δ-MnO_2 is not a separate mineral to Hx-birnessite: δ-MnO_2 is believed to be a Hx-birnessite in which the phyllomanganate sheets are incoherently stratified so that the ~7 and ~3.6 Å diffraction peaks are reduced in intensity (Manceau, pers. comm.). Vernadite is an alternative name for δ-MnO_2, while Fe-vernadite is typically a mixture of δ-MnO_2 and feroxyhite (δ-FeOOH) (Manceau and Combes 1988). The Fe^{3+} bearing phases in ferromanganese nodules and crusts are thought to be poorly ordered based on their weak and broad XRD patterns (e.g., Goodell et al. 1971; Burns and Burns 1977).

Ferromanganese nodules can be classified on the basis of their predominant Mn oxide. Nodules rich in todorokite are indicative of accretion influenced by oxic and sub-oxic early diagenetic reactions occurring in the sediment. As such, these are termed "diagenetic" nodules (e.g., Calvert and Price 1977). Nodules rich in δ-MnO_2 are indicative of accretion directly from the water column and are called "hydrogenetic" (e.g., Calvert and Price 1977). Todorkite-rich, diagenetic nodules show high Mn/Fe ratios whereas δ-MnO_2-rich, hydrogenetic nodules show low Mn/Fe ratios (e.g., Price and Calvert 1970; Jauhari 1987). Ferromanganese crusts form on exposed rock outcrops such as seamounts, topographically elevated areas, and volcanically active mid-ocean ridges; as such, there is no trace metal input from sediments. Ferromanganese crusts are classified as hydrogenetic at seamounts and hydrothermal at mid-ocean ridges (Cronan 1977). The main Mn mineral in hydrogenetic crusts is δ-MnO_2 (as Fe-vernadite, Koschinsky and Halbach 1995). The classification scheme outlined here is idealized: a gradation exists between hydrogenetic and hydrothermal crusts the closer they form to the hydrothermal source (e.g., Mills et al. 2001). Moreover, nominally hydrogenetic δ-MnO_2-rich nodules commonly accrete oxides from both the water column and sediments (Aplin and Cronan 1985), so that there is also a gradation between hydrogenetic and diagenetic nodules.

In the work described here, we determine the crystal chemistry of Ni associated with marine Mn oxides using EXAFS spectroscopy. We investigated a pristine hydrogenetic ferromanganese nodule (Madeira Abyssal Plain) and two Pacific Ocean ferromanganese hydrogenetic crusts. Hydrogenetic samples are of particular interest insofar as their chemistry reflects direct interaction with the water column.

Experimental methods

Samples

Two Pacific Ocean crust samples 79DSK4 (Location: 15°39'N, 170°24'W, Depth 2500 m) and 5DSR8 (Location 4°09'S, 174°54'W, Depth 1585 m) from Chu (2004) were studied. The crusts were collected from a seamount location and are therefore classified as hydrogenetic. These ferromanganese crusts consist predominantly (~60%) of Fe-Mn (hydr)oxides (Chu 2004) and bulk powdered samples, as supplied, were adequate for the objectives of the work done here. No further preparation was performed.

A pristine abyssal ferromanganese nodule from the Madeira Abyssal Plain was supplied by C. German, National Oceanography Centre, Southampton. Nodules are characteristically heterogeneous. Along with layers enriched in Fe-Mn (hydr)oxides, the interior typically consists of biogenic silica, phosphates, and carbonates. These commonly surround a core consisting of rock fragments and other detrital material. The nodule was encased in epoxyresin and sectioned with a wafering saw. One half was then ground using silicon carbide paper and dry polished using submicrometer alumina polishing powder so that we could visually identify regions of the nodule that are enriched in Fe-Mn(hydr)oxides. A well-defined, dark-colored rim was inferred to contain predominantly Fe-Mn (hydr)oxides.

SEM and EDS

Previous studies have shown a spatial correlation between Ni and Mn in Pacific and Indian Ocean ferromanganese nodules (e.g., Lei and Boström 1995 and Kumar et al. 1994, respectively). To corroborate this relation in our nodule from the North Atlantic, we measured the micro-spatial distribution of Ni, Fe, and Mn using EDS. We focused on the rim area of the nodule as this was visually identified (by the darker coloring) to be enriched in Fe-Mn (hydr)oxides. The polished nodule half was carbon-coated and a section of the rim analyzed in a Hitachi S-3500N scanning electron microscope (University of Bristol, Earth Science Department) equipped with an EDAX energy dispersive spectrometer (EDS). Accelerating voltage was 20 kV. The remaining nodule half was left unpolished and used for EXAFS analysis of the mirror image of the rim material studied with EDS (see below).

XRD

The mineralogy of the ferromanganese crusts and nodule rim section was identified using powder X-ray diffraction (XRD) with Cu$K\alpha$ radiation (using a Phillips PW1730 generator set to 40 kV and 20 mA). To achieve random orientation, packed powder mounts were used. Scans were done with a Phillips diffractometer using a 2θ step size of 0.1°, and samples were scanned from 5 to 70° with an integration time of 60 s per step.

The crust samples were obtained as powders and were analyzed in bulk. Since the well-defined dark rim of the nodule was inferred to contain predominantly Fe-Mn oxides, this was sampled to minimize contributions from clay minerals, carbonates, and phosphates. A sample of the rim material was removed from the freshly cut surface using a dental drill and ground to a fine powder using an agate pestle and mortar. XRD analysis (Fig. 1, see below) shows the nodule to be δ-MnO_2-rich and, as such, it can be classified as primarily hydrogenetic.

EXAFS data collection and analysis

EXAFS fluorescence spectra of the Ni *K*-edge (8333 eV) were collected on station 7.1 at the CLRC Synchrotron Radiation Source, Daresbury Laboratory, U.K. The unpolished, freshly exposed rim material of the nodule was presented to the X-ray beam by clamping the outer resin case and positioning the rim phase in the path of the X-ray beam. We analyzed the mirror image of the rim material extracted for XRD analysis from the polished nodule half. Pacific crust samples were presented to the beam as a dry powder held by cellophane tape in a 2 mm thick Teflon slide with a 4×15 mm sample slot. During data collection, storage ring energy was 2.0 GeV and the beam current varied between 130 and 240 mA. The monochromator was set to reject 30% of the incoming beam to minimize higher harmonics in the EXAFS spectrum. EXAFS spectra were obtained by summing up to 10 fluorescence mode scans obtained using an Ortec 18-element solid-state detector.

EXAFS data reduction was performed using Daresbury Laboratory software (EXCALIB and EXBACK, Dent and Mosselmans 1992). EXCALIB was used to calibrate from monochromator position (in millidegrees) into energy (eV) and sum

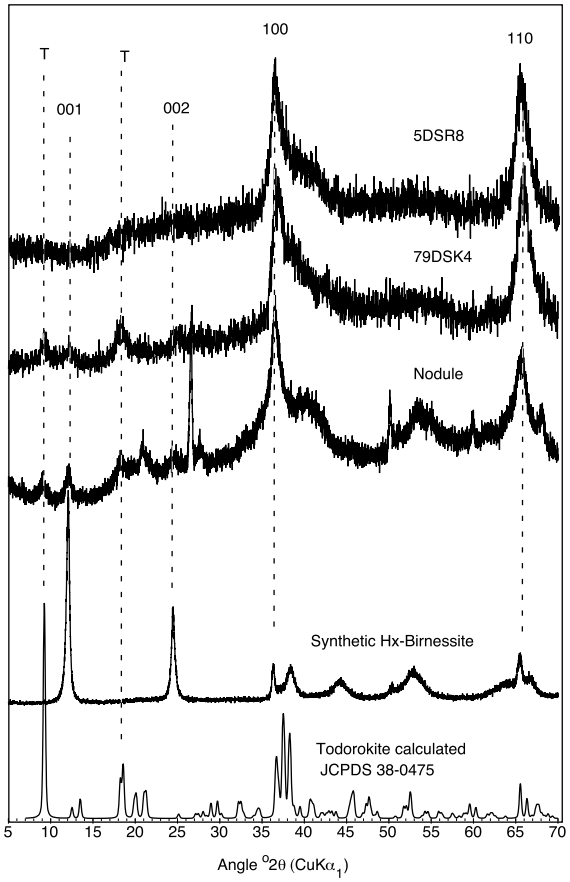

FIGURE 1. X-ray diffraction patterns for a synthetic Hx-birnessite, abyssal ferromanganese nodule and Pacific Ocean ferromanganese crusts showing 001, 002, 100, and 110 reflections of Hx-birnessite. Sharp peaks at 26.66, 50.18, and 60.00 °2θ are assigned to quartz. Peaks near 9 and 18 °2θ in the hydrogenetic nodule and 79DSK4 are probably due to poorly crystalline todorokite.

individual spectra. EXBACK was used to define the start of the EXAFS oscillations (determined from the inflection point on the K edge) and perform background subtraction. The pre-edge was fit to a linear function and the post-edge background to two 2nd-order polynomial segments. EXAFS were fit in the small atom approximation and we allowed for multiple scattering as coded in EXCURV98 (Binsted 1998). The three-dimensional coordination environment about the Ni atom was modeled using a cluster with C_3 symmetry (Fig. 2). This cluster allows for the full multiple scattering analysis with the smallest number of independent parameters. Lowering the symmetry to C_1 and treating each atom independently did not statistically improve the EXAFS fits. The phase-shift functions used in the curve fitting were derived by ab initio methods in EXCURV98 using Hedin-Lundqvist potentials (Hedin and Lundqvist 1969) and von Barth ground states. No Fourier filtering was performed during the data analysis.

RESULTS AND DISCUSSION

Mineralogy and crystallinity

XRD patterns of the ferromanganese nodule and Pacific Ocean ferromanganese crusts samples are shown in Figure 1 and compared to that of a synthetic Hx-birnessite (Peacock and Sherman 2007). Characterization of $Mn^{3+/4+}$ and Fe^{3+} minerals in ferromanganese deposits by diffraction methods is difficult because of their poor crystallinity, yielding only a few broad peaks, and indicating the presence of multiple $Mn^{3+/4+}$ and Fe^{3+} (hydr)oxides. Todorokite is usually characterized by first- and second-order basal diffraction peaks corresponding to ~10 and ~4.8 Å *d*-spacings, respectively. Birnessites (including both Tc-birnessite and Hx-birnessite) are characterized by basal diffraction peaks corresponding at ~7–7.2 Å (001) and 3.5–3.6 Å (002). These reflections signify ordered stacking of the octahedral sheets with an interlayer separation equal to 7–7.2 Å (Drits et al. 1997). Broad *hk* bands at ~2.4 and ~1.4 Å are also present. These bands arise from 100 (~2.4 Å) and 110 (~1.4 Å) reflections. Hx-birnessite is identified by $d_{100}/d_{110} = \sqrt{3}$. A sample is identified as δ-MnO_2 when the (001) and (002) reflections of Hx-birnessite are weak or absent (i.e., only the broad *hk* bands at ~2.4 and 1.4 Å can be seen). Of the Fe^{3+}-bearing minerals, goethite and lepidocrocite are characterized by first-, second-, and third-order basal diffraction peaks corresponding to 4.18, 2.45, and 2.69 Å *d*-spacings (goethite ICDD 29-0713), and 6.26, 3.29, and 2.47 Å *d*-spacings (lepidocrocite ICDD 08-0098). Feroxyhyte (see Manceau and Combes 1988) has X-ray lines corresponding to *d*-spacings of 2.54, 2.22, 1.69, and 1.47 Å (Carlson and Schwertmann 1980).

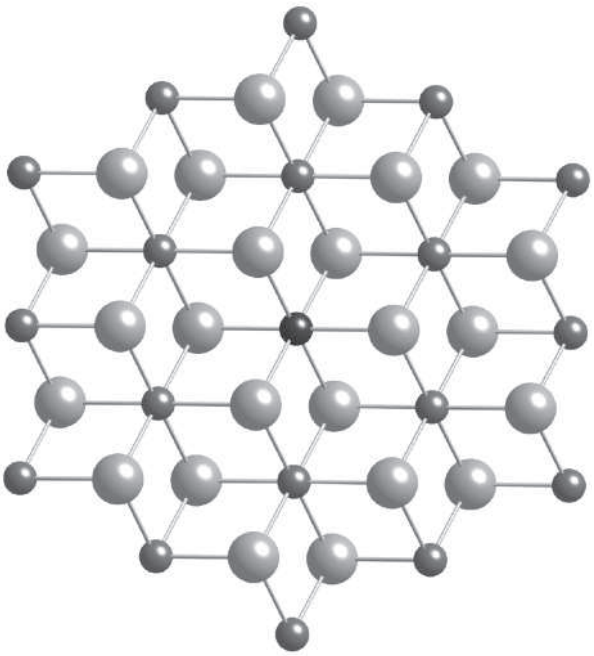

FIGURE 2. Cluster used in EXAFS fits for Ni^{2+} sorbed to Pacific Ocean ferromanganese crust and abyssal ferromanganese nodule.

The XRD pattern of the ferromanganese nodule rim sample shows phase that is poorly crystalline relative to the synthetic Hx-birnessite (Fig. 1). XRD diffraction peaks at ~7.2 and ~3.5 Å indicate the presence of birnessite, while $d_{100}/d_{110} = \sqrt{3}$ is indicative of hexagonal symmetry. Peaks corresponding to *d*-spacings at ~2.22 and ~1.69 Å (and 2.54 and 1.47 Å contained within the broad *hk* band peaks at ~2.4 and ~1.4 Å, respectively) suggest the presence of feroxyhyte. Feroxyhyte is most likely associated with δ-MnO_2 in the nodule (Manceau and Combes 1988). Small peaks corresponding to *d*-spacings ~10 and ~4.8 Å mean we can-

not rule out the presence of some poorly crystalline todorokite in the rim phase of our ferromanganese nodule. Quartz is also present as indicated by the sharp reflections at 26.66, 20.88, 50.18, and 60.00 °2θ.

The XRD patterns of the Pacific Ocean ferromanganese crust samples also show a phase that is poorly crystalline relative to synthetic Hx-birnessite (Fig. 1). For samples 5DSR8 and 79DSK4, the broad XRD peaks corresponding to d-spacings at ~2.4 and ~1.4 Å indicate the presence of δ-MnO_2. This identification is in agreement with several mineralogical studies of hydrogenetic crusts (e.g., Koschinsky and Hein 2003). Small peaks corresponding to *d*-spacings at ~10 and ~4.8 Å in sample 79DSK4 indicate the possible presence of some poorly crystalline todorokite.

Elemental mapping of ferromanganese nodule

EDS maps of Fe, Mn, and Ni in the ferromanganese nodule rim are shown in Figure 3. The Fe and Mn scans show typical interlamination (e.g., Dutta et al. 2001) of Fe-rich and Mn-rich phases; Mn-enriched layers are associated with Fe-depleted ones. The Mn and Ni scans show a positive Mn-Ni spatial correlation consistent with previous sequential extraction analyses (e.g., Aplin and Cronan 1985) and SEM of Indian Ocean deposits (e.g., Dutta et al. 2001). Specific Ni-Mn hot-spots (regions a and b in Fig. 3) are ~100 μm in diameter. The Fe concentrations in areas a and b are low (Fig. 3); this finding is consistent with a positive Ni correlation with Mn and its anti-correlation with Fe as observed by Dutta et al. (2001).

EXAFS spectroscopy

Ni *K*-edge EXAFS (and Fourier transforms of the EXAFS) for Pacific Ocean crusts and ferromanganese nodule shown in Figure 4 and summarized in Table 1. In both the Pacific Ocean crusts (79DSK4 and 5DSR8) and ferromanaganese nodule, we find that Ni is surrounded by 6 O atoms at ~2.0 and 6 Mn at ~2.9 Å. We interpret this result to indicate that Ni^{2+} replaces $Mn^{3+/4+}$ in the phyllomanganate layer of a phase similar to Hx-birnessite (e.g., δ-MnO_2). To verify this interpretation, we fit the EXAFS data using the cluster shown in Figure 2 and included full multiple scattering. We find that, indeed, the cluster is able to account for the apparent shells at distances up to 5 Å with minimal refinement from the theoretical bond distances and bond angles expected from the Hx-birnessite structure. The coordination environment of Ni in the ferromanganese crust and nodule is distinguishable from that of Ni^{2+} in $Ni(OH)_2$ insofar as the latter phase has 6 Ni-Ni distances at 3.13 Å and 2 Ni-Ni distances at 4.63 Å. Sorption of Ni in todorokite is not believed to be significant in these samples since todorokite is only a minor component (if present) and the next-nearest neighbor Mn distances would include shells at 3.5–3.6 Å resulting from corner-sharing between NiO_6 and MnO_6 octahedra.

The substitution of Ni for Mn in a phyllomanganate layer can

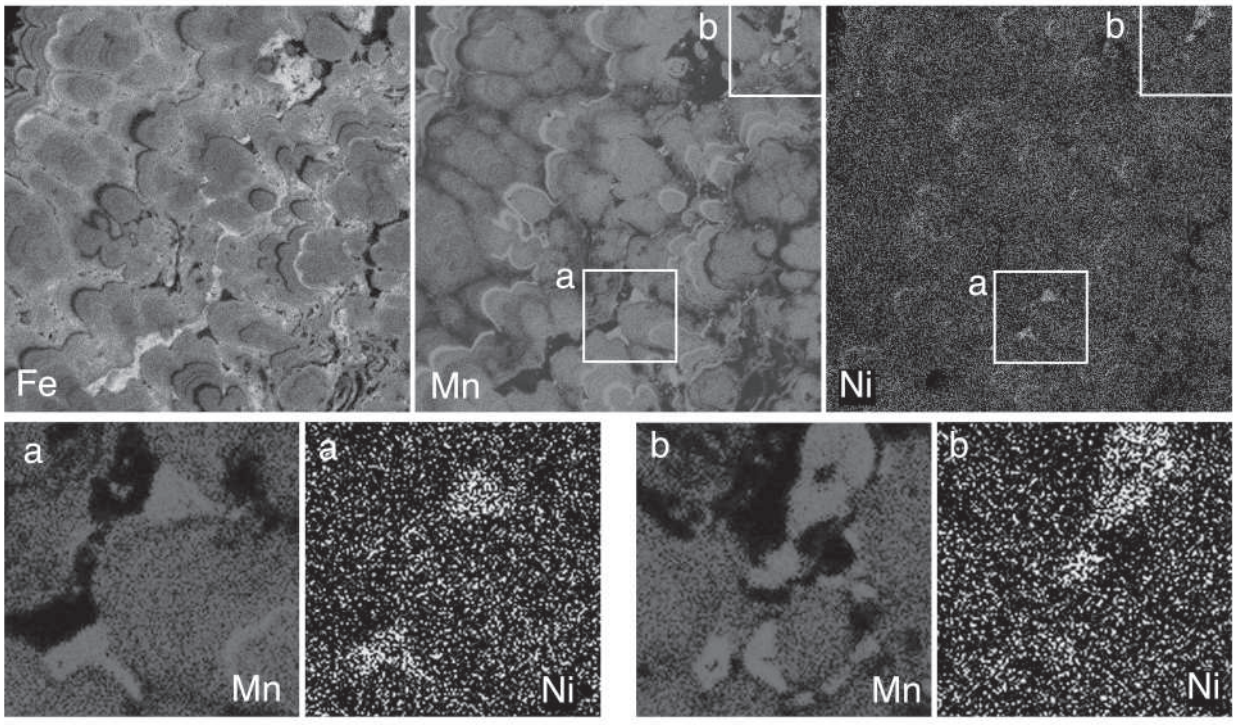

FIGURE 3. EDS elemental maps of a selected area (scan size = 2.35 × 2.35 mm) in the outer rim of the ferromanganese nodule. Lighter areas indicate higher elemental concentration. Iron and Mn scans show typical interlamination of Fe- and Mn-rich phases with a negative Fe-Mn spatial correlation. Nickel is concentrated in regions high in Mn and low in Fe. Expanded regions of high Ni and Mn concentration ("a" and "b") are shown in the bottom images.

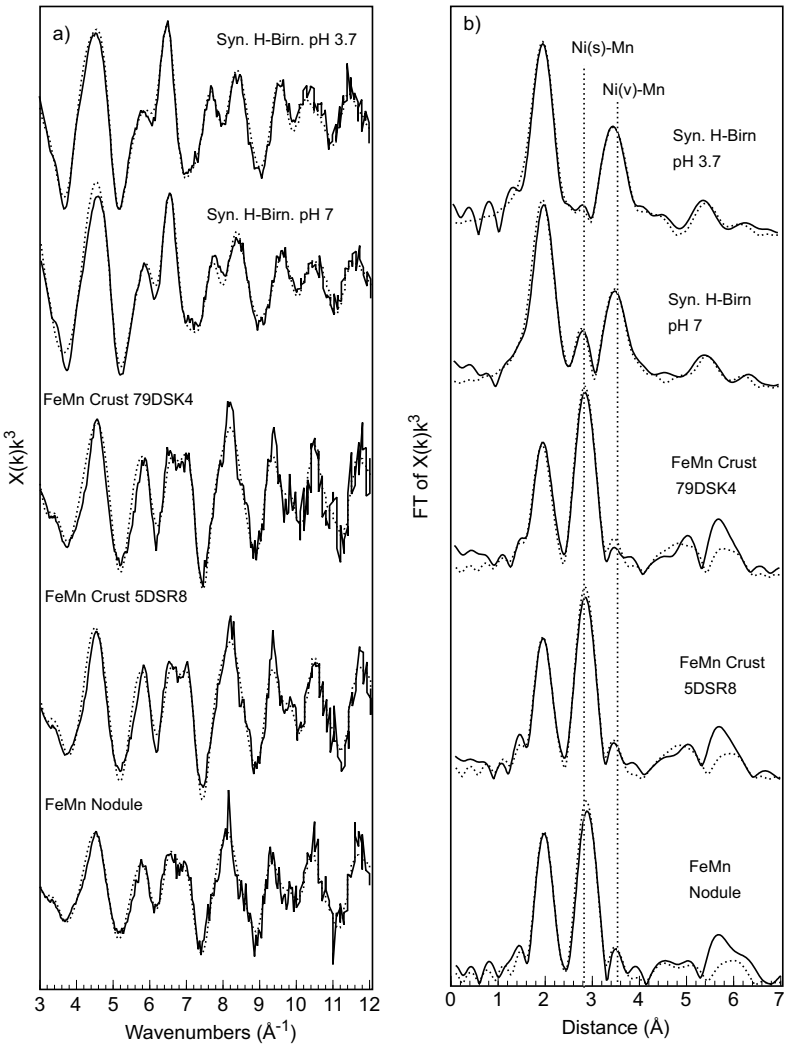

FIGURE 4. (**a**) EXAFS and (**b**) Fourier transform of EXAFS for Ni^{2+} on Pacific Ocean ferromanganese crusts and abyssal ferromanganese nodule samples. Also shown are EXAFS of Ni sorbed to synthetic H-birnessite (Peacock and Sherman 2007) at pH 3.7 and 7. Ni(s)-Mn refers to the Ni-Mn distance expected for Ni substituting for Mn in the phyllomanganate layer. Ni(v)-Mn refers to the Ni-Mn distance expected for Ni sorbed above vacancy sites in the phyllomanganate layer.

TABLE 1. Structural parameters for the cluster (C_3 symmetry) used to model EXAFS fits for Ni^{2+} in Pacific Ocean ferromanganese crust and abyssal ferromanganese nodule

	N	R in Å	θ	Φ	$2\sigma^2$ in Å^2
FeMn Crust 5DSR8					
Ni_0	*1.0*	0.00	*0*	*0*	0.000
O_1	*3.0*	2.06	47.0	*0*	0.010
O_2	*3.0*	2.00	135.6	*180*	0.007
Mn_3	*3.0*	2.83	*90*	*270*	0.010
Mn_4	*3.0*	2.88	*90*	*90*	0.008
Mn_5	*3.0*	5.92	*90*	*270*	0.007
Mn_6	*3.0*	4.93	*90*	*180*	0.007
Mn_7	*3.0*	5.04	*90*	*0*	0.007
Mn_8	*3.0*	5.91	*90*	*90*	0.008
O_9	*3.0*	3.35	105.0	*0*	0.007
O_{10}	*3.0*	3.50	75.0	*180*	0.008
O_{11}	*3.0*	4.55	75.6	*105*	0.007
O_{12}	*3.0*	4.52	105.0	*45*	0.007
O_{13}	*3.0*	4.52	100.0	*75*	0.008
O_{14}	*3.0*	4.47	75.0	*135*	0.007
FeMn Crust 79DSK4					
Ni_0	*1.0*	0.00	*0*	*0*	0.000
O_1	*3.0*	2.04	47.0	*0*	0.010
O_2	*3.0*	2.00	135.6	*180*	0.010
Mn_3	*3.0*	2.83	*90*	*270*	0.010
Mn_4	*3.0*	2.87	*90*	*90*	*0.010*
Mn_5	*3.0*	5.88	*90*	*270*	0.006
Mn_6	*3.0*	4.94	*90*	*180*	0.010
Mn_7	*3.0*	5.00	*90*	*0*	0.008
Mn_8	*3.0*	5.91	*90*	*90*	0.007
O_9	*3.0*	3.22	105.0	*0*	0.010
O_{10}	*3.0*	3.42	75.0	*180*	0.010
O_{11}	*3.0*	4.41	75.6	*105*	0.005
O_{12}	*3.0*	4.56	105.0	*45*	0.009
O_{13}	*3.0*	4.48	100.0	*75*	0.008
O_{14}	*3.0*	4.50	75.0	*135*	0.006
FeMn Nodule					
Ni_0	*1.0*	0.00	*0*	*0*	0.000
O_1	*3.0*	2.02	47.0	*0*	0.008
O_2	*3.0*	2.03	135.6	*180*	0.004
Mn_3	*3.0*	2.86	*90*	*270*	0.009
Mn_4	*3.0*	2.86	*90*	*90*	0.009
Mn_5	*3.0*	5.94	*90*	*270*	0.006
Mn_6	*3.0*	4.91	*90*	*180*	0.009
Mn_7	*3.0*	5.04	*90*	*0*	0.010
Mn_8	*3.0*	5.91	*90*	*90*	0.006
O_9	*3.0*	3.33	105.0	*0*	0.010
O_{10}	*3.0*	3.49	75.0	*180*	0.010
O_{11}	*3.0*	4.45	75.6	*105*	0.007
O_{12}	*3.0*	4.53	105.0	*45*	0.007
O_{13}	*3.0*	4.50	100.0	*75*	0.007
O_{14}	*3.0*	4.57	75.0	*135*	0.007

Notes: N = the number of atoms in each shell, was constrained by symmetry. σ is the Debye-Waller factor; R, θ, and φ are the spherical coordinates of the prototype atom in each shell with C_3 symmetry. Angular values in italics were also fixed.

be contrasted with the surface complexation of freshly sorbed Ni on synthetic Hx-birnessite. In the latter, Ni sorbs by forming tridentate inner-sphere surface complexes over the octahedral vacancies in Hx-birnessite (Peacock and Sherman 2007). This is indicated by the Ni-Mn distance of 3.5 Å (Fig. 4) and is expected based on previous studies of metal sorption to synthetic Hx-birnessite (Manceau et al. 2002a). However, the EXAFS spectrum of synthetic Hx-birnessite at pH 7 (Fig. 4) shows that some Ni is sorbed by structural incorporation as indicated by the Ni-Mn distance near 2.9 Å. In a companion study (Peacock and Sherman 2007), we were able to model this spectrum as a linear combination of the coordination environments of Ni in the natural Hx-birnessite (sample 5DSR8) and the synthetic Hx-birnessite at pH 3.7. This approach indicates that ~10 % of the Ni has been structurally incorporated into synthetic Hx-birnessite at pH 7. Further work is needed to understand the energetics of surface complexation vs. structural incorporation and the consequences for reversible uptake of Ni by marine ferromanganese oxides.

ACKNOWLEDGMENTS

Helpful comments which improved the manuscript were provided by an anonymous reviewer and the associate editor. Thanks are due to Stuart Kearns and Remmert Schouten (University of Bristol) for assistance with SEM and XRD sample preparation, respectively. We are especially grateful to Jon Wade (University of Bristol) for his help with SEM sample preparation and analysis. We also thank Chris Corrigan (Daresbury Phases Support Laboratory) for XRD, and Fred Mosslemans (Daresbury Laboratory) for support at Station 7.1. We are especially grateful to Chris German (NOCS, Southampton, U.K.) for providing the ferromanganese nodule and Pacific crust samples, and Alain Manceau (University of Grenoble) for valuable discussion on the interpretation of Mn oxide XRD patterns.

C.L.P. was supported by a NERC studentship. Beamtime for EXAFS spectroscopy was provided by CLRC.

REFERENCES CITED

Aplin, A.C. and Cronan, D.S. (1985) Ferromanganese oxide deposits from the Central Pacific Ocean, II. Nodules and associated sediments. Geochimica et Cosmochimica Acta, 49, 437–451.

Binsted, N. (1998) EXCURV98: The manual. Daresbury Laboratory, Warrington, U.K.

Brown, G.E. and Parks, G.A. (2001) Sorption of trace elements on mineral surfaces: Modern perspectives from spectroscopic studies, and comments on sorption in the marine environment. International Geology Review, 43, 963–1073.

Burns, R.G. and Burns, V.M. (1977) Mineralogy. In G.P. Glasby, Ed., Marine manganese deposits, p. 186–248. Elsevier oceanographic series 15, Elsevier, Amsterdam.

Calvert, S.E. and Price, N.B. (1977) Geochemical variation in ferromanganese nodules and associated sediments from the Pacific Ocean. Marine Chemistry, 5, 43–74.

Carlson, L. and Schwertmann, U. (1980) Natural occurrence of feroxyhyte (δ-FeOOH). Clays and Clay Minerals, 28, 272–280.

Catts, J.G. and Langmuir, D. (1986) Adsorption of Cu, Pb and Zn by δMnO_2: applicability of the site binding-surface complexation model. Applied Geochemistry, 1, 255–264.

Chu, N-C. (2004) An investigation into Hf and Fe isotopes in ferromanganese deposits and their applications to paleoceanography, p. 208. Ph.D. thesis, University of Southampton, U.K.

Cronan, D.S. (1969) Inter-element associations in some pelagic deposits. Chemical Geology, 5, 99–106.

——— (1977) Deep-sea nodules: distribution and geochemistry. In G.P. Glasby, Ed., Marine manganese deposits, p. 11–44. Elsevier oceanographic series 15, Elsevier, Amsterdam.

Dent, A.J. and Mosselmans, J.F.W. (1992) A guide to EXBACK, EXCALIB and EXCURV92. CLRC Daresbury Laboratory, Warrington, U.K.

Drits, V.A., Silvester, E., Gorshkov, A.I., and Manceau, A. (1997) Structure of synthetic monoclinic Na-rich birnessite and hexagonal birnessite: I. Results from X-ray diffraction and selected-area electron diffraction. American Mineralogist, 82, 946–961.

Dutta, R.K., Sideras-Haddad, E., and Connell, S.H. (2001) Distribution of various components in a hydrogenous ferromanganese nodule and an Afanasiy Nikitin Seamount crust from Indian Ocean—A geochemical study using micro-PIXE. Nuclear Instruments and Methods in Physics Research B, 181, 545–550.

Giovanoli, R. (1980) On natural and synthetic manganese nodules. In J.M. Varenstov and J. Grasselly, Eds., Geology and geochemistry of manganese, 1, p. 154–202. Academia Kiado, Budapest.

Goldberg, E.D. (1954) Marine Geochemistry I—Chemical scavengers of the sea. Journal of Geology, 62, 249–265.

Goodell, H.G., Meylan, M.A., and Grant, B. (1971) Ferromanganese deposits of the South Pacific Ocean, Drake Passage, and Scotia Sea. Antarctic Research Series, 15, 27–92.

Hedin, L. and Lundqvist, S. (1969) Effects of electron-electron and electron-photon interactions on the one-electron states of solids. Solid State Physics, 23, 1–181.

James, R.D. and Healy, T.W. (1972) Adsorption of hydrolyzable metal ions at the oxide-water interface III. A thermodynamic model of adsorption. Journal of Colloid and Interface Science, 40, 65–81.

Jauhari, P. (1987) Classification and inter-element relationships of ferromanganese nodules from the Central Indian Ocean Basin. Marine Minerals, 6, 419–429.

Jones, L.H.P. and Milne, A.A. (1956) Birnessite, a new manganese oxide mineral from Aberdeenshire, Scotland. Mineralogical Magazine, 31, 283–288.

Koschinsky, A. and Halbach, P. (1995) Sequential leaching of marine ferromanganese precipitates: Genetic implications. Geochimica et Cosmochimica Acta, 59, 5113–5132.

Koschinsky, A. and Hein, J.R. (2003) Uptake of elements from seawater by ferromanganese crusts: solid-phase associations and seawater speciation. Marine Geology, 198, 331–351.

Kumar, R., Das, S.K., Ray, R.K., and Biswas, A.K. (1994) A SEM backscattered electron mode study of microstructural features of ferromanganese nodules from central Indian Ocean basin. Transactions of the Indian Institute of Metals, 47, 273–285.

Lei, G. and Boström, K. (1995) Mineralogical control on transition metal distributions in marine manganese nodules. Marine Geology, 123, 253–261.

Li, Y.-H. (1982) Interelement relationship in abyssal Pacific ferromanganese nodules and associated pelagic sediments. Geochimica et Cosmochimica Acta, 46, 1053–1060.

Manceau, A. and Combes, J.M. (1988) Structure of Mn and Fe oxides and oxyhydroxides: a topological approach by EXAFS. Physics and Chemistry of Minerals, 15, 283–295.

Manceau, A., Gorshkov, A.I., and Drits, V.A. (1992) Structural chemistry of Mn, Fe, Co, and Ni in manganese hydrous oxides: Part II. Information from EXAFS spectroscopy and electron and X-ray diffraction. American Mineralogist, 77, 1144–1157.

Manceau, A., Lanson, B., and Drits, V.A. (2002a) Structure of heavy metal sorbed birnessite. Part III: Results from powder and polarized extended X-ray absorption fine structure spectroscopy. Geochimica et Cosmochimica Acta, 66, 2639–2663.

Manceau, A., Tamura, N., Marcus, M.A., MacDowell, A.A., Celestre, R.S., Sublett, R. E., Sposito, G., and Padmore, H.A. (2002b) Deciphering Ni sequestration in soil ferromanganese nodules by combining X-ray fluorescence, absorption and diffraction at micrometer scales of resolution. American Mineralogist, 87, 1494–1499.

Manceau, A., Tommaseo, C., Rihs, S., Geoffroy, N., Chateigner, D., Schlegel, M., Tisserand, D., Marcus, M.A., Tamura, N., and Chen, Z-S. (2005) Natural speciation of Mn, Ni, and Zn at the micrometer scale in a clayey paddy soil using X-ray fluorescence, absorption and diffraction. Geochimica et Cosmochimica Acta, 69, 4007–4034.

McKenzie, R.M. (1989) Manganese oxides and hydroxides. In J.B. Dixon and S.B.Weed, Eds., Minerals in soil environments, p. 493–502. Soil Science Society of America, Madison, Wisconsin.

Mills, R.A., Wells, D.M., and Robert, S. (2001) Genesis of ferromanganese crusts from the TAG hydrothermal field. Chemical Geology, 176, 283–293.

Moorby, S.A. and Cronan, D.S. (1981) The distribution of elements between coexisting phases in some marine ferromanganese-oxide deposits. Geochimica et Cosmochimica Acta, 45, 1855–1877.

Peacock, C.L. and Sherman, D.M. (2007) Sorption of Ni by birnessite: equilibrium controls on Ni in Seawater. Chemical Geology, 238, 94–106.

Post, J.E. (1992) Crystal structures of manganese oxide minerals. In H.C.W. Skinner and R.W. Fitzpatrick, Eds., Biomineralization processes: Iron, manganese, p. 51–73. Catena Supplement 21, Catena, Cremlingen-Destedt, Germany.

Price, N.B. and Calvert, S.E. (1970) Compositional variation in Pacific Ocean ferromanganese nodules and its relationships to sediment accumulation. Marine Geology, 9, 145–171.

Turner, D.R., Whitfield, M., and Dickson, A.G. (1981) The equilibrium speciation of dissolved components in freshwater and seawater at 25 °C and 1 atm pressure. Geochimica et Cosmochimica Acta, 45, 855–881.

Usui, A. (1979) Nickel and copper accumulation as essential elements in 10-Å manganite of deep-sea manganese nodules. Nature, 279, 411–413.

Villalobos, M., Toner, B., Bargar, J., and Sposito, G. (2003) Characterization of the manganese oxide produced by Pseudomonas putida strain MnB1. Geochimica et Cosmochimica Acta, 67, 2649–2662.

Willis, J.P. and Ahrens, L.H. (1962) Some investigations on the composition of manganese nodules with particular reference to certain trace elements. Geochimica et Cosmochimica Acta, 26, 751–764.

MANUSCRIPT RECEIVED JULY 4, 2006
MANUSCRIPT ACCEPTED MARCH 3, 2007
MANUSCRIPT HANDLED BY LAURENCE GARVIE